ERJ
Engineering Research Journal
Faculty of Engineering
Minoufiya University

THEORETICAL ANALYSIS OF COOLING EFFECT ON THE EFFECTIVENESS OF GAS TURBINE BLADES

M. Khalil Bassiouny, S. A. Wilson and M. F. Mosa

Mechanical Power Engineering Department
Faculty of Engineering, Minoufiya University, Shebin El-Kom, Egypt
Mfam133@yahoo.com

ABSTRACT

The modern gas turbine engines operate at high pressure ratio and consequently higher entry turbine temperatures. At high loads, this temperature exceeds the allowable metal-temperature limits. The turbine blades need to be protected to ensure their integrity. The efficient cooling technique such as film cooling is therefore essential to protect the gas turbine blades. The efficiency of this technique depends on several parameters, such as the injection blowing ratio, density ratio, mainstream turbulence intensity, mainstream pressure gradient, boundary layer thickness, injection angle, spacing between holes as well as their arrangement, and the blade geometry. The main objective of this study was to make a numerical study on the first stage for both profiles VKI and C3X turbine blades cascade with a leading edge showerhead film-cooling arrangement by using the commercial code Fluent v. 5.4. The governing equations for steady, two-dimensional, turbulent, compressible flow are integrated over arbitrary two-dimensional control volumes with the aid of Gauss theorem. The present computational model seeks to a realistic film-cooled turbine blade. The code is used to study the combination of film and convection cooling. While most of the theoretical studies considered isothermal blade surfaces in thermal calculations over the blade surfaces. The results indicated that the film cooling enhances adiabatic effectiveness and decreases the surface heat flux by six times that of uncooling blade. In case of increasing the blowing ratios or streamwise injection angle, the adiabatic effectiveness decreases gradually. The effectiveness for combined cooling is higher than that of film cooling only due to the combination of film and convection cooling together. Also the film cooling effectiveness for the VKI profile is higher than that of the C3X profile as a result of the better design shape of VKI profile. The model had been validated and tested with previously published experimental and theoretical results. These comparisons show a satisfactory agreement that permits an extension of the theoretical study.

تستخدم التربينات الغازية في العديد من المجالات مثل الطائرات والسفن الحربية والصواريخ ومحطات توليد الطاقة الكهربائية. ولزيادة الكفاءة الحرارية يجب رفع درجة حرارة الغازات الساخنة عند مدخل التربينة إلى قيم تتخطى ١٨٠٠ درجة مئوية. إلا أن هذه الحرارة العالية تتسبب باجهادات حرارية عالية ينتج عنها انهيار أو تشوه ريش التربينة. وتعتبر ريش التوجيه في مرحلة التمدد الأولى بالتربينة الأكثر تعرضا لدرجة الحرارة العالية الأمر الذي يتطلب تركيز الاهتمام بالتبريد على هذه الريش. وللتغلب على هذه المشكلة فقد تم تطوير عدة طرق لتبريد ريش التربينة وزيادة عمرها الافتراضي ومن أهم هذه الطرق التبريد الطبقي والذي تعتمد فكرته على حقن كتلة من الهواء من خلال ثقوب موزعة على سطح الريشة مكونا طبقة من الهواء البارد والذي يعزل سطح الريشة عن الغازات الساخنة. و قد تناول هذا البحث بالدراسة النظرية تأثير التبريد على الخصائص الأيروديناميكية وانتقال الحرارة لريش التوجيه في التربينة الغازية لتقييم أداء التبريد وإيضاح العوامل المختلفة المؤثرة على إجراء التبريد ومدى تأثيرها على فاعليته، لذلك فقد تم صياغة نموذج رياضي لدراسة سريان الغازات خلال شكلين مختلفين من ريش التربينة الغازية و هما VKI & C3X. كما تم استخدم طريقتين من طرق التبريد و هما : التبريد الطبقي والتبريد المزدوج (تبريد داخلي + تبريد سطحي)،، وقد تم تغيير كلا من نسبة و زاوية حقن هواء التبريد وشدة السريان الاضطرابي. وقد تم إستخدام النموذج الرياضي لدراسة تأثيرات عوامل التشغيل المختلفة على أداء التبريد. وقد أوضحت النتائج النظرية التي تم الحصول عليها أن التبريد الطبقي يحسن من كفاءة التبريد ويقلل من انتقال الحرارة بمقدار ست مرات. كما تبين من الدراسة أن زيادة كلا من نسبة و زاوية الحقن يقلل من كفاءة التبريد. كما أظهرت النتائج أن كفاءة التبريد للريشة من النوع VKI أعلى من كفاءة التبريد للريشة من النوع C3X، و أن كفاءة التبريد المزدوج (تبريد طبقي + تبريد داخلي) تكون أعلى من كفاءة التبريد الطبقي فقط.

Keywords: Film cooling, Effectiveness, Gas turbine, Nozzle blades.

1. INTRODUCTION

Over the past fifty years, aircraft and power generation gas turbine designers have endeavored to increase the combustor exit and high-pressure turbine stage inlet temperature. With higher combustor exit temperatures, improved efficiency and reduced fuel consumption can be achieved. Modern gas turbine engines are designed to operate at inlet temperatures of 1800-2000°C, which are far beyond the allowable metal temperature. Unfortunately, these higher temperatures have a negative effect on the integrity of the high-pressure turbine components and specifically the turbine blades. Thus to maintain acceptable life and safety standards, the structural elements need to be protected against the severe thermal environment. To achieve that, researchers focus on various innovative cooling techniques. This life may be reduced by 50% if the blade's operating temperature was above the maximum design temperature by 10°C.

The review of the previous investigations on film cooling for gas turbine applications are presented and discussed. Those investigations are divided into two groups:

i – Film Cooling Flow on a Flat Plate

Early studies were made by Andreopoulos et al. [1] performed a preliminary experimental investigation of film cooling over flat plate. The results indicated that immediately after penetration into the mainstream flow the jet behaves like a flexible body. At some distance from the jet exit, two counter-rotating vortices are formed which produce the classic 'kidney' shape of the injection. The creation of these vortices is connected to viscous layers in the injection tube. Richard et al. [2] provided an experimental investigation of film cooling flow with lateral injection. Azzi et al. and Goldstein et al. [3-4] conducted theoretical and experimental investigations on the effect of injection angle over flat plate. They found that the compound angle injection provides a better film-cooling protection than the simple angle injection for the same blowing ratio. Baldauf et al. [5] carried out an experimental investigation to compute the adiabatic film-cooling effectiveness, heat transfer coefficient and the resulting heat flux reduction due to film cooling on a flat plate surface by means of infrared thermography. James et al. [6] provided an experimental investigation studying the effects of freestream turbulence on adiabatic effectiveness on a film-cooled flat plate. The results indicated that high freestream turbulence has little effect on effectiveness for a blowing ratio of Br = 1.5, but makes the effectiveness worse for blowing ratio of Br = 0.5. Michael et al. and Christian et al. [7,8] investigated three different shapes: (i) round, (ii) latterly diffused, and (iii) forward-latterly diffused. The film effectiveness of case (iii) was significantly higher than others. At the same time, the heat transfer coefficient was high for round shape holes. The reason for getting lower (h) for expanded holes is the spread out of the jets laterally. Trent [9] carried out an experimental study on a flat plate to investigate the film cooling effectiveness through measurements of four different techniques: steady-state liquid crystal, transient liquid crystal, pressure sensitive paint, and thermocouples. The study focused then on the film cooling performance of various shaped film cooling holes in comparison to the reference geometry of cylindrical holes with a compound angle. They found that all methods except for the transient liquid crystal showed the same effectiveness data for the higher blowing ratios. Compound angles increase the lateral momentum of the coolant which provides better coverage in the spanwise direction. The conical shaped holes had the worst effectiveness performance.

ii – Film Cooling Flow on a Blade

Early studies were made by Hall et al. [10]. They performed a preliminary numerical investigation of film cooling over realistic C3X airfoils. Garg et al. [11] predicted a three-dimensional Navier-Stokes code to study the effect of coolant temperature, and coolant to mainstream mass flow rate ratio on the adiabatic effectiveness of a film-cooled turbine blade. They found that on the pressure side of shower-head holes, the effectiveness decreases with increase in coolant mass flow due to coolant jet lift-off. Friedrichs [12] conducted a comprehensive investigation of the endwall film-cooling. The results of their study indicated a strong influence of the secondary flows on the film-cooling. Their data showed that the angle at which the coolant leaves the hole did not dictate the coolant trajectory except near the hole exit. Guo et al. [13] carried out experimental study using the thin-film technology to measure the heat transfer coefficient and cooling effectiveness over nozzle guide blades. The results indicated a scatter of data for both the film cooling effectiveness and the heat transfer coefficient profiles. The explanation for the strange profiles was that the coolant film lifted off the blade surface. James [14] predicted experimentally the relationship between the plenum to freestream total pressure ratio on film cooling performance. Results showed that the heat transfer coefficient is independent of the pressure ratio. Also, a weak reduction of film cooling effectiveness with higher pressure ratios is obtained. Youn et al. and Vijay et al. [15-16] studied experimentally the performance of film cooling by shaped injection holes for the turbine blade leading edge region. The results showed that the conventional cylindrical holes have poor film cooling performance compared to the shaped holes.

Theodoridis et al. and Traverso et al. [17-18] predicted a three-dimensional calculation of the compressible flow field around a turbine blade with film cooling injection near the leading edge.

2. MATHEMATICAL MODEL

The compressible turbulent flow inside blade-to-blade passage was predicted by solving numerically the two dimensional continuity, momentum and energy equations. The analysis is based on an implicit finite volume method to discretize the flow domain in the relevant transport equations. The (k-ε) turbulence model is used to close up the system of the momentum differential equations. In order to account for the compressibility effects, the equation of state and up-winding scheme is used to interpolate the density at control volume faces. Discretize the governing equations of fluid flow results in a system of linear algebraic equations, which are solved by tri-diagonal matrix algorithm (TDMA).

2.1. Governing Equations

The general form of two-dimensional steady viscous and compressible flow governing equations of mass and momentum can be written in Cartesian coordinates as:

- Continuity Equation:

$$\frac{\partial}{\partial x_j}\left(\rho U_j\right) = 0 \qquad (1)$$

- Momentum Equation:

$$\frac{\partial}{\partial x_j}\left(\rho U_j U_i\right) = -\frac{\partial P}{\partial x_i} + \frac{\partial}{\partial x_j}\left(\mu_e \frac{\partial U_i}{\partial x_j}\right) \qquad (2)$$

- Turbulence kinetic energy k:

$$\frac{\partial}{\partial x_j}\left(\rho U_j k\right) = G - C_d \rho\varepsilon + \frac{\partial}{\partial x_j}\left(\Gamma_k \frac{\partial k}{\partial x_j}\right) \qquad (3)$$

- Energy dissipation rate ε :

$$\frac{\partial}{\partial x_j}\left(\rho U_j \varepsilon\right) = C_1 \frac{\varepsilon}{k} G - C_2 \frac{\rho\varepsilon^2}{k} + \frac{\partial}{\partial x_j}\left(\Gamma_\varepsilon \frac{\partial \varepsilon}{\partial x_j}\right) \qquad (4)$$

The turbulent viscosity is computed according to

$$\mu_t = \rho C_\mu \frac{k^2}{\varepsilon} \qquad (5)$$

The production term G_k is

$$G = \mu_t \left\{ 2\left[\left(\frac{\partial u}{\partial x}\right)^2 + \left(\frac{\partial v}{\partial y}\right)^2\right] + \left(\frac{\partial u}{\partial y} + \frac{\partial v}{\partial x}\right)^2 \right\} \qquad (6)$$

The empirical values of turbulent constants are: $C_1 = 1.44$; $C_2 = 1.92$; $C_\mu = 0.09$; $\sigma_k = 1.0$; $\sigma_\varepsilon = 1.3$

$$;\Gamma_\varepsilon = \frac{\mu_e}{\sigma_\varepsilon} \quad ; \quad \Gamma_k = \frac{\mu_e}{\sigma_k}$$

- Energy Equation:

$$\frac{\partial}{\partial x_j}\left(\rho U_j h\right) - \frac{\partial}{\partial x_j}\left(\Gamma_h \frac{\partial h}{\partial x_j}\right) = 0 \qquad (7)$$

Where $\Gamma_h = \frac{\mu}{\mathrm{Pr}} + \frac{\mu_t}{\mathrm{Pr}_t}$; $h = C_p.T$

- State Equation :

$$P = \rho RT \qquad (8)$$

2.2. Assumptions

In order to adopt an applicable computational method, some assumptions are made:

1. The entering fluid flow is a perfect gas, Newtonian, uniform, turbulent and compressible.
2. The fluid flow is steady, adiabatic, ir-rotational, single-phase, and shock free.

2.3. Grid System

A single-block grid approach is adopted to model this complex geometry, in which a system of locally unstructured grid block is generated as in Fig. (1). This single-block system is generated in the present study by the grid generation program Gambit. This program produces a body-fitted single -block grid with triangular cells and full face-matching block as in Fig. (2). The grid is composed of 98168 computational cells.

2.4. Boundary Conditions

The turbine first stage nozzle blade of this study is based on an Allied-Signal film cooled engine design and called VKI and C3X profiles. The freestream inlet flow to the blade is at an angle of 0 deg. At the main flow inlet boundary located at an axial distance equal to 80% of the blade axial chord upstream of the blade leading edge, the total temperature, total pressure, Mach number and turbulence intensity are 2000 K , 29.14 bar, 0.5 and 5.0% respectively. At the main flow exit plane located at an axial distance equal to 70% of the blade axial chord downstream of the blade trailing edge, the exit static temperature and pressure values are 1970 K and 22.48 bar, respectively. At the solid surfaces of the blade, plenum and hole-pipes, the no-slip condition is enforced, and the wall temperatures ratio, $T_w/T_g = 0.62$. The blade was internally cooled by an array of nine radial cooling holes which feed by one plenum. The cold fluid at T_{c1} = 740 K enters through the plenum chamber with a constant value of Br. The model dimensions are in meter, and the fluid properties and boundary conditions are given in SI units.

2.5. Model Verification

In order to extend the theoretical study process of film cooling problems, the model must be firstly validated. The results of the present model are compared with published experimental and analytical results of [19, 20, 21 and 22]. The Dimensions of the computational grid used in the numerical simulations in ref. [19] is shown in Fig. (3). These comparisons are presented in Figs. (4) to (6) using the data of ref. [19] under the same conditions of motive velocity, temperature, and turbulence intensity of the mainstream gas, as well as temperature, angle of injection, blowing ratio of the cooling jet. While the comparison presented in Figs. (8) to (14) is done under the same conditions of motive stagnation pressure and temperature, P_o & T_o through the tested VKI and C3X profiles. Blade cascade design parameters and turbine blade flow conditions are described in Tables 1, 2, 3, 4 and 5 respectively. The comparisons show acceptable agreement that permits an extension of the theoretical study.

3. RESULTS AND DISCUSSIONS

3.1. Effect of Aerodynamics Parameters

This section concerns with studying the effect of aerodynamics parameters on the film cooling performance. These parameters are blowing ratio and turbulence intensity. The effect of each parameter is investigated separately at different given values of the other parameters. In the investigated nozzle blade, the blade true chord length (C), axial chord length (C_{ax}), blade span (H), and blade pitch (Pi) are 120, 87, 72 and 96 mm respectively. The inlet flow angle (B1) and exit flow angle (B2) are 0oand 70o respectively. The holes locations (s/c) from hole 1 to 9 are 0.0, -0.0226, -0.05388, -0.08416, 0.0226, 0.061696, 0.18368, 0.26733 and -0.38456 respectively.

3.1.1. Effect of blowing ratio Br on film cooling

Effect of blowing ratio on external surface adiabatic effectiveness distribution on the nozzle blade is shown in Fig. (15). In pressure side and with increasing Br the gas from the freestream has migrated to the blade surface due to lift off the coolant jet from the blade surface. The coolant jet is thus no longer effective in cooling the surface. This is due to the secondary flow within the coolant jet, and the resulting entrainment of the hot gas from the outer region towards the airfoil surface between the adjacent jets. The lift-off is a jet crossflow interaction based upon pressure fields and momentum balances. The penetration of the coolant jet from the shower-head holes depends mainly on the injection angle, the momentum ratio $(\rho v^2)_c/(\rho v^2)_g$ and the pitch-to-diameter ratio. While the injection angle and pitch-to-diameter ratio were kept constant, the momentum ratio was varied in the present study. As the coolant mass flow increases further, the coolant jet lifts off sooner and the jets penetrate deeper into the freestream and the vortices are lifted further from the surface. It is clear from Fig. (15) that when Br = 8%, the coolant traces lift-off the pressure surface, and after some distance the coolant jet reattach the pressure surface as described before. But in suction side at low coolant mass flow (Br = 8%), the coolant covers the blade surface well and remains fairly attached to the blade surface due to the low coolant mass flow ratio.

Figure (16) presents the external heat flux for a wall temperature of T_w = 1118 K. It should be noticed that the external heat flux may be either positive (heat flux into fluid) or negative (heat flux into solid) because the wall temperature is between the freestream and coolant temperatures. The largest heat flux occurs along the stagnation line, between rows 1 and 2, where coolant is absent, but this occurs over a very short streamwise distance. Presence of negative values of q_w at some locations simply implies that the direction of heat transfer is from fluid to blade at these locations due to specification of the isothermal wall boundary condition and film temperature. This illustrates the dependence of wall heat flux on wall temperature. At low blowing ratios the coolant jet is attached to the pressure surface so that the temperature difference between the blade surface and fluid will be positive and hence the heat flux is transferred from solid to fluid.

Figure (17) shows the effect of blowing ratio on drag and lift coefficients. The x-abscissa represents blowing ratio and the y-abscissa represents drag and lift coefficients. The drag and lift coefficients are calculated as follows,

$$c_d = \frac{F_d}{\frac{\rho_{in} \cdot u_{in}^2}{2} \cdot C} \quad ; \quad c_L = \frac{F_L}{\frac{\rho_{in} \cdot u_{in}^2}{2} \cdot C}$$

Where: F_d and F_L are the drag and lift forces respectively, ρ_{in}, u_{in} are the density and velocity of the freestream at inlet and C is the blade chord.

With increasing Br the drag and lift coefficients will decrease. As the coolant mass flow increases further, the coolant jet lifts off sooner, the jets penetrate deeper into the freestream, the vortices are lifted further from the surface and the secondary flow within the coolant jet will increase also. So that the pressure fields over pressure and suction surface will decrease as a result of interaction between jets and cross flow.

3.1.2. Effect of free-stream turbulence Tu on film cooling

Since the flow in a gas turbine engine typically has freestream turbulence on the order of 10–20% in the regions where film cooling is employed. It is

important to study how this freestream turbulence affects film cooling performance. The effect of turbulence intensity, Tu is investigated separately at different given values of the blowing ratio.

3.1.2.1. Effect of free-stream turbulence at low blowing ratios

Figure (18) shows the effect of freestream turbulence at low blowing ratios, Br = 0.08, on external surface adiabatic effectiveness distribution on the nozzle blade. The x-abscissa represents the surface distance along the blade chord. The y-abscissa represents the adiabatic effectiveness. In pressure and suction side for a low value of Tu = 5 and low Br, the cooling air remains near the surface and cools it well.

3.1.2.2. Effect of free-stream turbulence at high blowing ratios

Figure (19) illustrates the effect of freestream turbulence Tu at a high blowing ratios, Br = 0.18, on external surface adiabatic effectiveness distribution on the nozzle blade. In case of low Tu and high Br, the cooling air lifts off from the surface as it leaves the hole, and therefore it has a bad effect. High Tu mixes the lifted off air and bring some of it back near the surface, improving the effectiveness. When high freestream turbulence is introduced Tu = 20, it removes much of this cooling air from the near surface and mixes it with the freestream, resulting in less cooling air near the surface and therefore lower effectiveness is obtained.

Briefly, with increasing Tu the gas from the freestream has migrated to the blade surface due to lift off the coolant jet from the blade surface. The coolant jet is thus no longer effective in cooling the surface. This is due to the secondary flow within the coolant jet, and the resulting entrainment of the hot gas from the outer region towards the airfoil surface between the adjacent jets. The jet lifts off and counter-rotating vortices entrain hot gases from the mainstream to the wall surface. The jet being detached from the wall, the hot gases can reach the wall. The lift-off is a jet crossflow interaction based upon pressure fields and momentum balances and freestream turbulence.

Figure (20) indicates the effect of freestream turbulence Tu at low and high blowing ratios, Br = 0.08 and 0.18, on drag and lift coefficients on the nozzle blade. The x-abscissa represents the freestream turbulence Tu and the y-abscissa represents the drag and lift coefficients. In case of low Br, with increasing Tu the drag and the lift coefficients will decrease gradually. For high Br case, with increasing Tu the drag and the lift coefficients will decrease more than that at low Br. As the freestream turbulence increases further, the vortices are lifted further from the surface and the secondary flow within the coolant jet will increase also. So, the pressure fields over pressure and suction surface will decrease as a result of interaction between jets and cross flow.

3.2. Effect of Geometric Parameters

3.2.1. Effect of geometric parameters, α_j

There are a number of geometric parameters that affect the performance of film cooling such as cooling holes locations, hole length, hole arrangement, and blowing angle. The most influential parameter is the injection angle.

Figure (21) shows the external adiabatic effectiveness distribution on the nozzle blade. The x-abscissa represents the surface distance along the blade chord and the y-abscissa represents the adiabatic effectiveness.

In pressure side and with increasing the streamwise injection angle the gas from the freestream has migrated to the blade surface due to lift off the coolant jet from the blade surface. The lift-off is a jet crossflow interaction based upon pressure fields, momentum balances, and streamwise injection angle. The penetration of the coolant jet from the shower-head holes depends mainly on the injection angle, on the momentum ratio $(\rho v^2)_c/(\rho v^2)_g$ and on the pitch-to-diameter ratio. While the momentum ratio and pitch-to-diameter ratio were kept constant, the injection angle was varied in the present study. As the injection angle increases further, the coolant jet lifts off sooner and the jets penetrate deeper into the freestream and the vortices are lifted further from the surface so that the adiabatic effectiveness will be smaller.

It is clear from figure that when $\alpha_j = 70°$, the coolant traces lift-off the pressure surface, and after some distance the coolant jet reattach the pressure surface as described before. When the injection angle increases further so that $\alpha_j = 110°$, the coolant traces lift-off the pressure side earlier, leading to higher adiabatic wall temperature and thus lower η on the pressure side at leading edge.

Figure (22) explains external heat flux distribution on the nozzle blade for a wall temperature of $T_w = 1118$ K. The x-abscissa represents the surface distance along the blade normalized by axial chord and the y-abscissa represents the heat flux. The largest heat flux occurs along the stagnation line, between rows 1 and 2, where coolant is absent, but this occurs over a very short streamwise distance. With increasing α_j the gas from the freestream has migrated to the blade surface due to lift off the coolant jet from the blade surface. The coolant jet is thus no longer effective in cooling the surface. This is due to the secondary flow within the coolant jet, and the resulting entrainment of the hot gas from the outer region towards the airfoil surface between the adjacent jets so that the heat flux will increase.

k	Turbulent kinetic energy, m^2/s^2
Ma	Mach number
Nu	Nusselt number {Nu = $h.C_{ax} / \lambda$}
P	Pressure, Pa
P_{rt}	Turbulent Prandtl number
R	Gas constant, J/kg.K
Re	Reynolds number based on the true chord length (Re= $\rho_g U_g C/\mu$)
S	Distance from the leading edge along the pressure or suction surface(streamwise distance from leading edge) , m
St	Stanton number {St =h/ ($\rho U_g Cp$)}
T	Temperature, K
Tu	Turbulence intensity
U_c	Coolant velocity at the hole exit, m/s
U_g	Approach mainstream velocity, m/s
x,y,z	Coordinate in the streamwise, pitchwise, and spanwise direction respectively, m

6.2. Greek symbols:

η	Adiabatic effectiveness, $(T_g - T_{aw}) /(T_g - T_c)$
η_{cc}	Combination cooling effectiveness (film plus convection cooling)
α_j	Streamwise (injection) film hole angle w.r.t the local blade surface
β	Spanwise film hole angle w.r.t the local blade surface
ε	Dissipation rate,m^2/s^3
λ	Gas thermal conductivity, W/m.K
μ	Dynamic viscosity, Pa.s
μ_t	Turbulent viscosity
ν	Kinematic viscosity, m^2/s

6.3. Subscripts

aw	Adiabatic wall
c	Plenum supply conditions
ex	Value at exit of the stator passage
g	Freestream (main flow) inlet conditions
o	Stagnation conditions
w	Wall

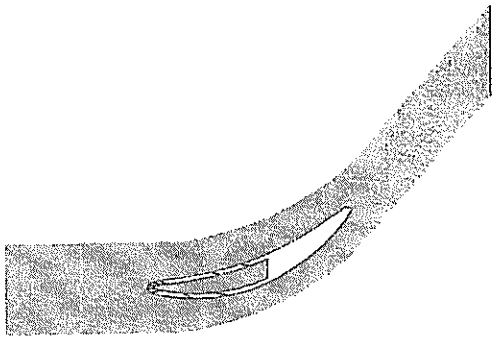

Fig.(1-a) The Triangular Grid for the nozzle blades cascade.

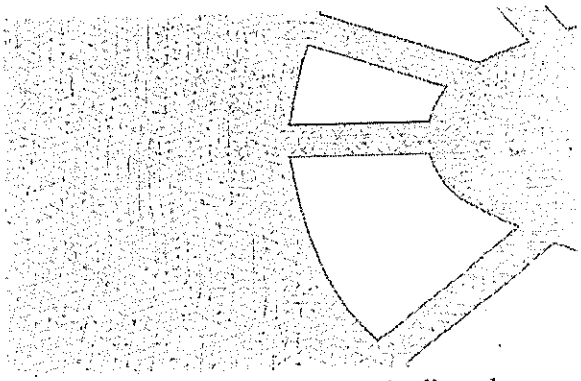

Fig.(1-b) Magnifier section at leading edge.

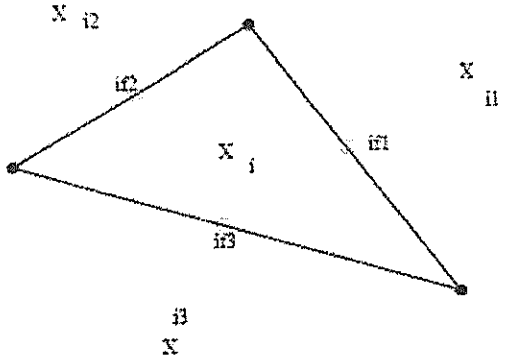

Fig. (2) A triangular control volume i with its three neighbours il, i2 and i3.Grid points are marked with black dots (•), cell centers with X, s, and cell faces with open circles.

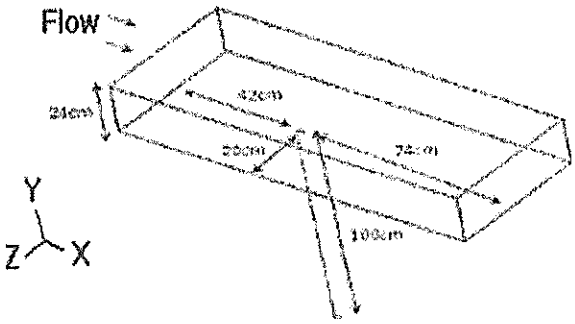

Fig. (3) Dimensions of the computational grid used in the numerical simulations, d = 2.35 cm.

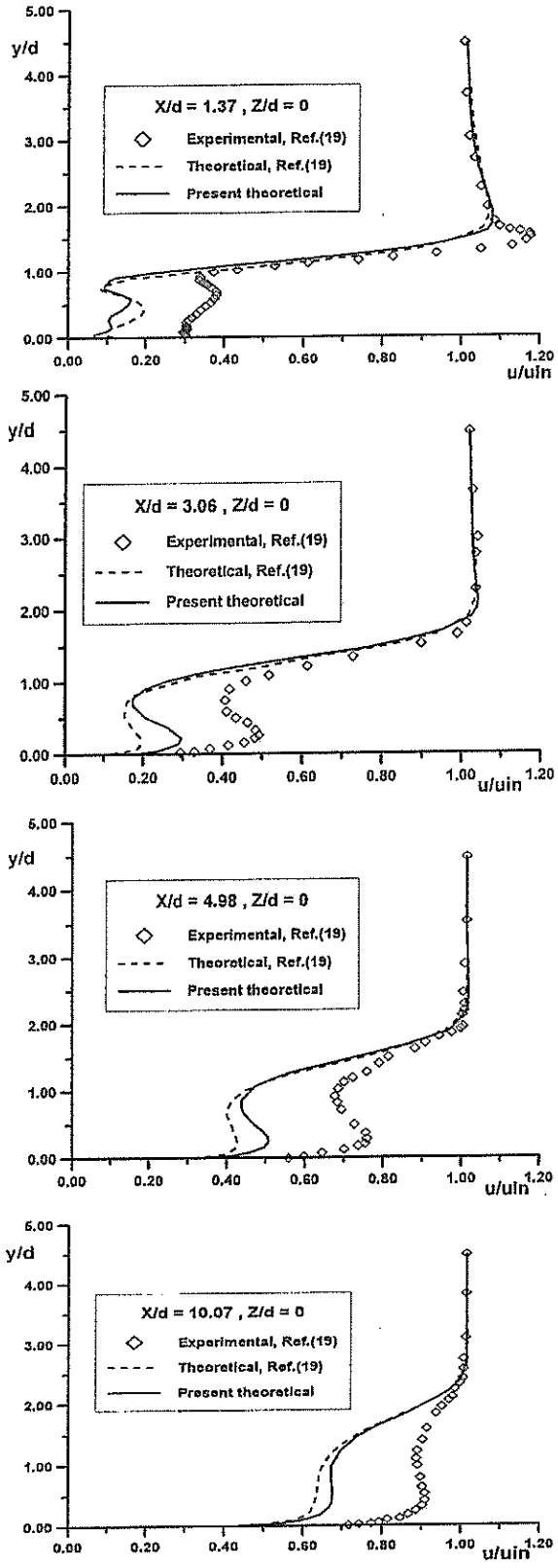

Fig. (4) Comparison between predicted variation of axial magnitude velocity and published theoretical and experimental data, ref. [19], at four axial locations.

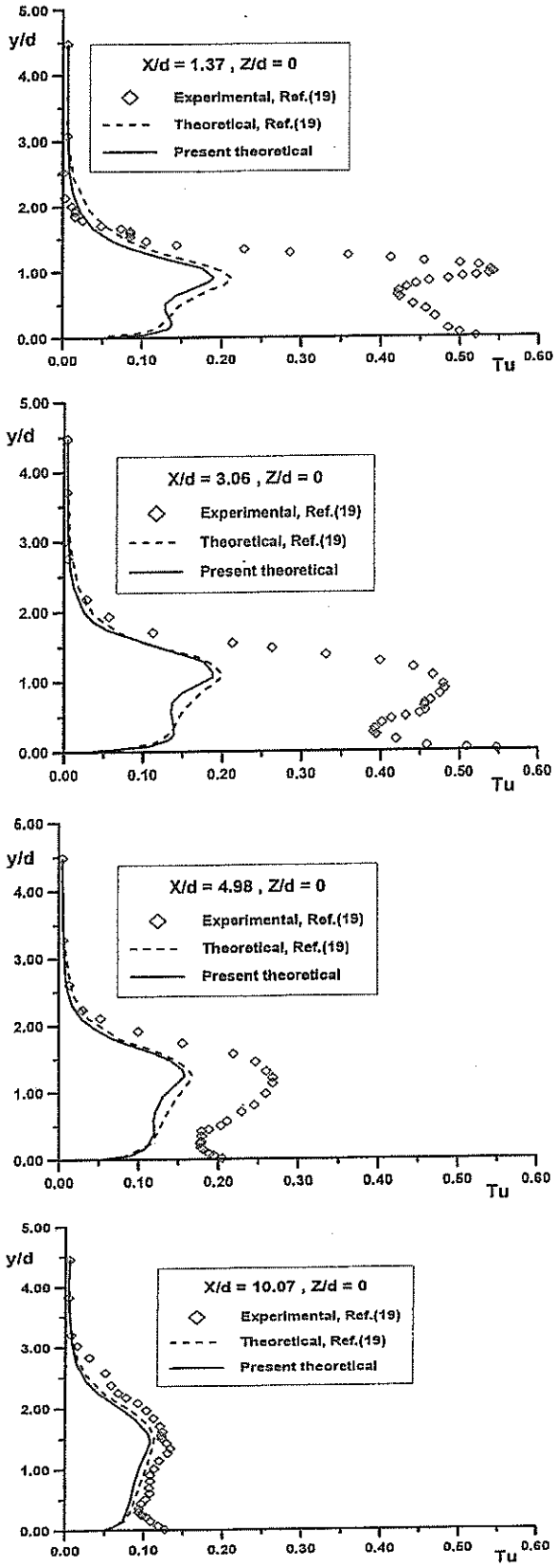

Fig. (5) Comparison between predicted variation of turbulence intensity and published theoretical and experimental data, ref. [19], at four axial locations.

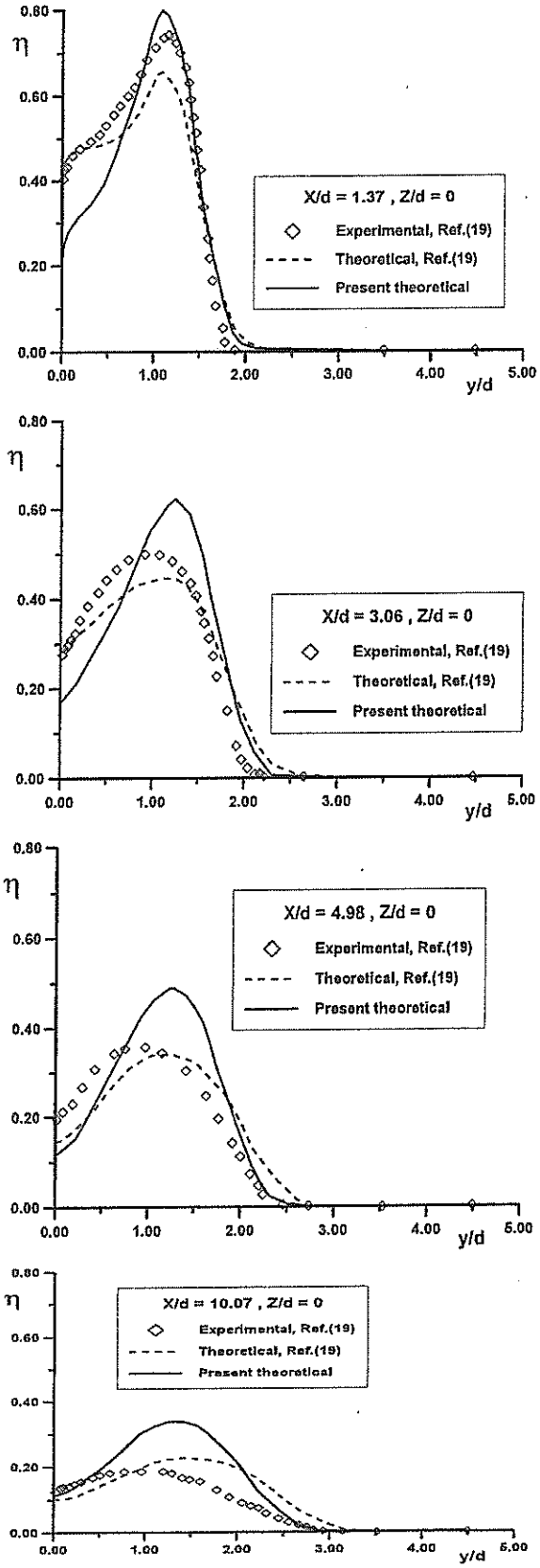

Fig. (6) Comparison between predicted variation of film effectiveness and published theoretical and experimental data, ref. [19], at four axial locations.

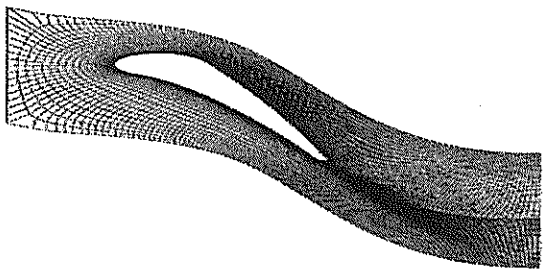

Fig. (7) Meshing grid for the nozzle blades.

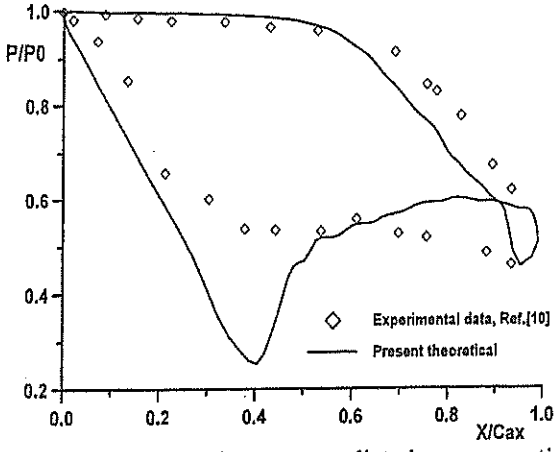

Fig.(8) Comparison between predicted pressure ratio and Published experimental data, ref. [10].

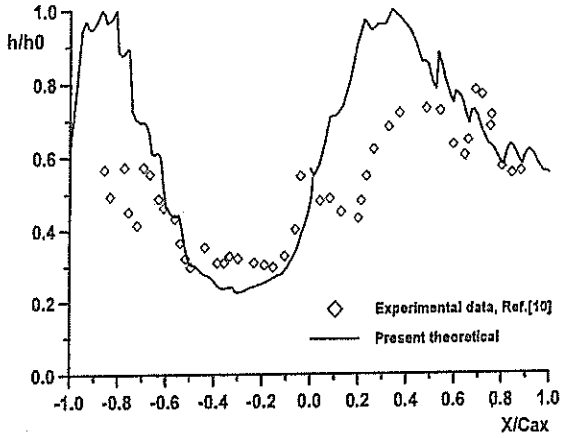

Fig. (9) Comparison between predicted heat transfer coefficient and Published experimental data, ref. [10].

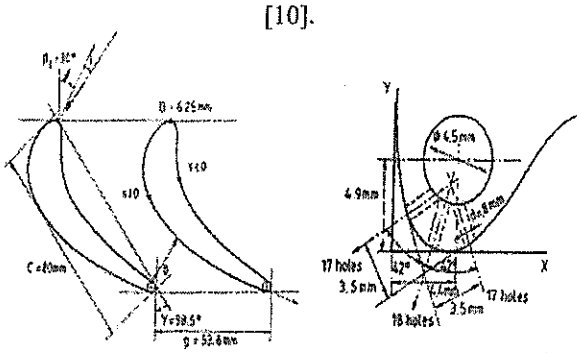

Fig.(10) VKI profile and shower head cooling hole details.

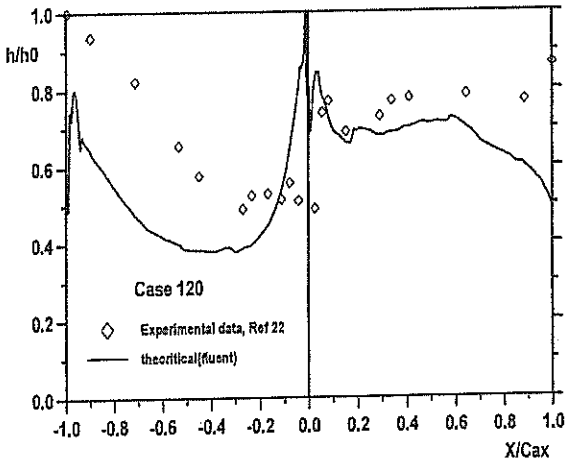

Fig.(11) Comparison between predicted heat transfer coefficient and Published experimental data, ref. [22].

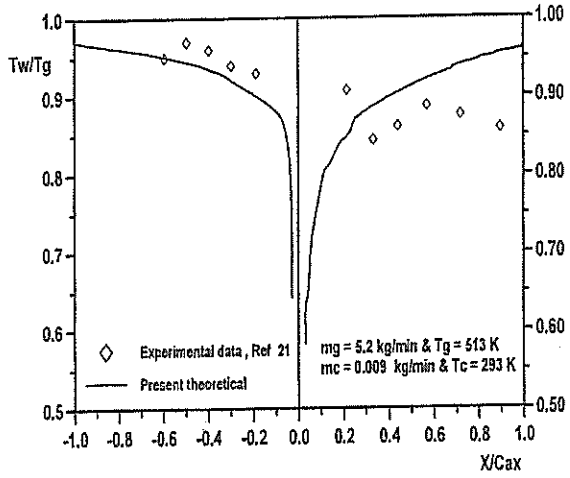

Fig.(12) Comparison between predicted local blade wall to gas temperature ratio and Published experimental data, ref. [21].

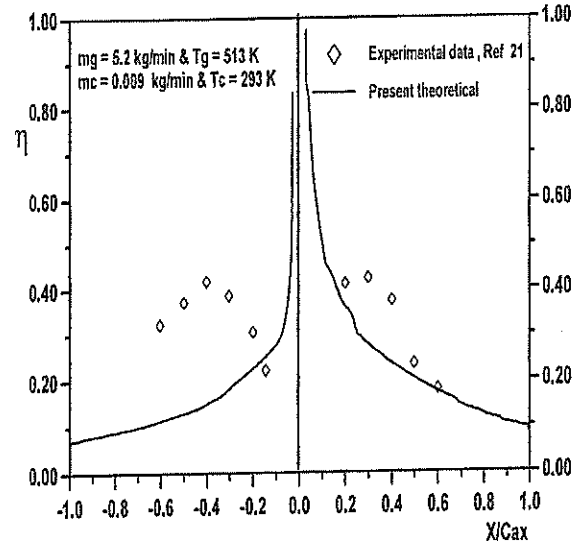

Fig.(13) Comparison of cooling effectiveness on the blade wall with experimental data, ref. [21].

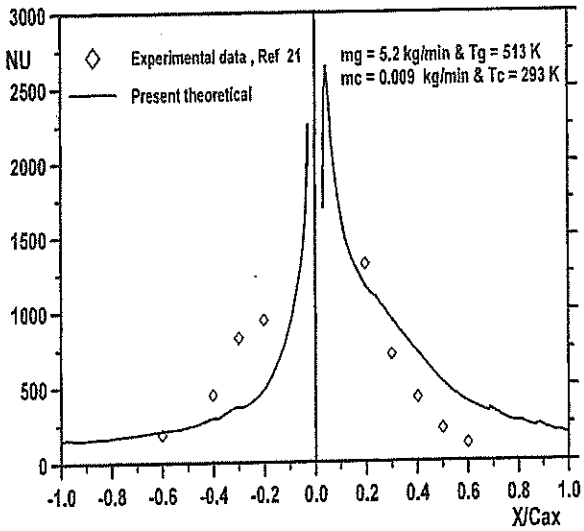

Fig.(14) Comparison between predicted Nusselt number and Published experimental data, ref [21].

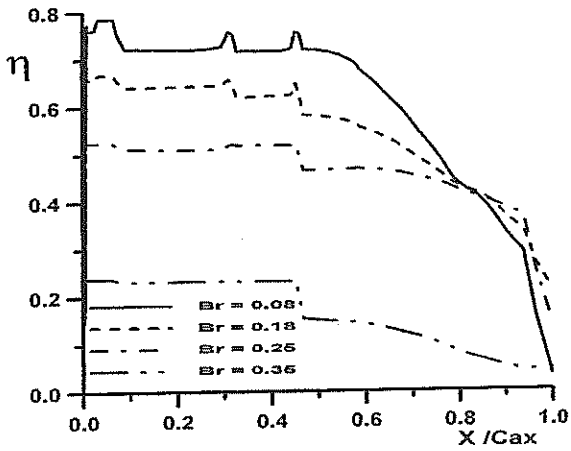

Fig.(15) Effect of blowing ratio on the film-cooling effectiveness distribution over blade wall, Tu = 5.

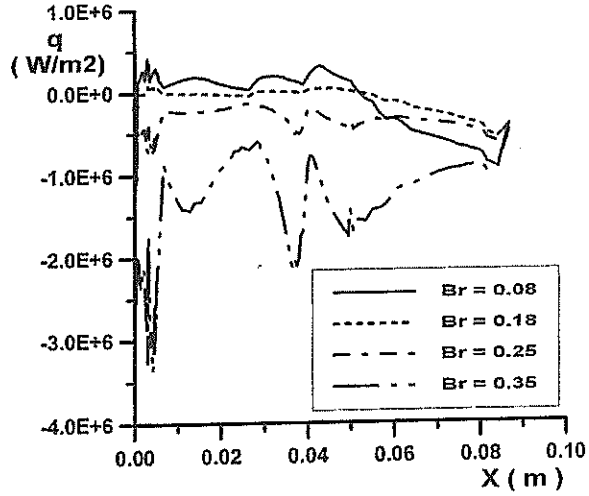

Fig.(16) Effect of blowing ratio on heat flux distribution over nozzle blade wall, Tu = 5, T_w/T_g = 0.62.

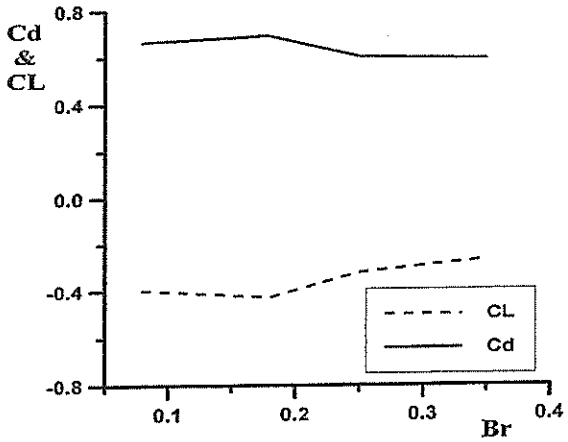

Fig.(17) Effect of blowing ratio on drag and lift coefficients, Tu = 5, T_w/T_g = 0.62.

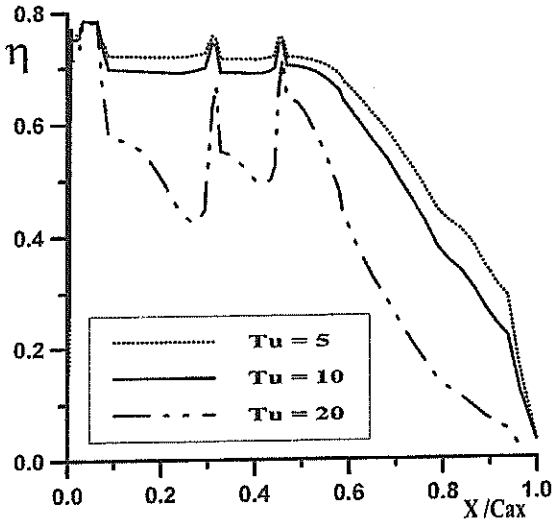

Fig.(18) Effect of freestream turbulence on the film-cooling effectiveness at Br = 0.08.

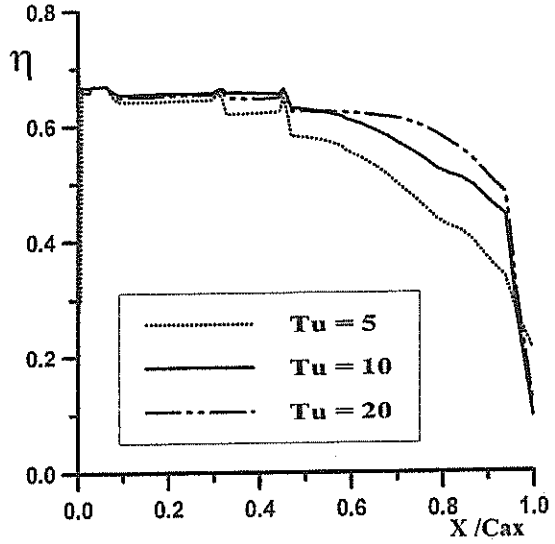

Fig.(19) Effect of freestream turbulence on the film-cooling effectiveness at Br = 0.18.

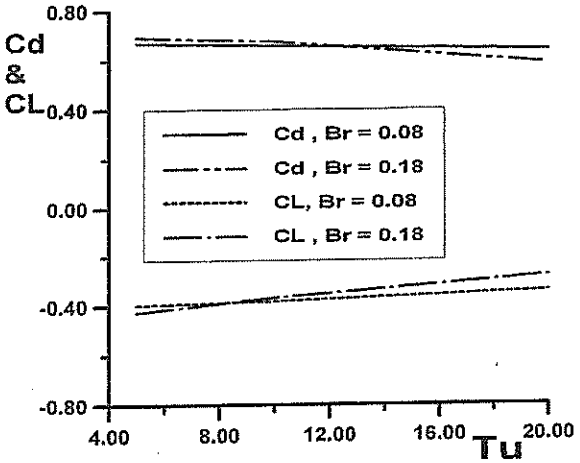

Fig.(20) Effect of freestream turbulence on drag and lift coefficients, Br = 0.08 and 0.18.

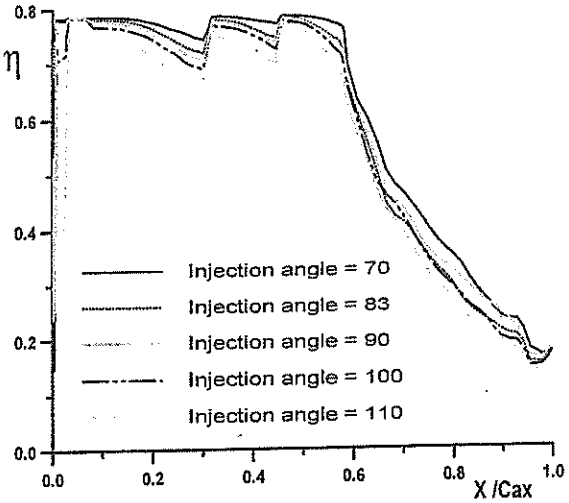

Fig. (21) Effect of injection angle on the film cooling effectiveness, Br = 0.08, Tu = 5 %.

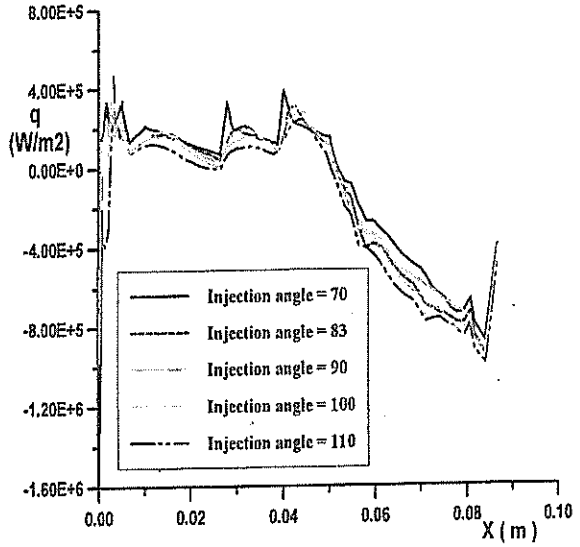

Fig. (22) Effect of injection angle on heat flux distribution over blade wall, T_w/T_g = 0.62, Br = 0.08, Tu = 5 %.

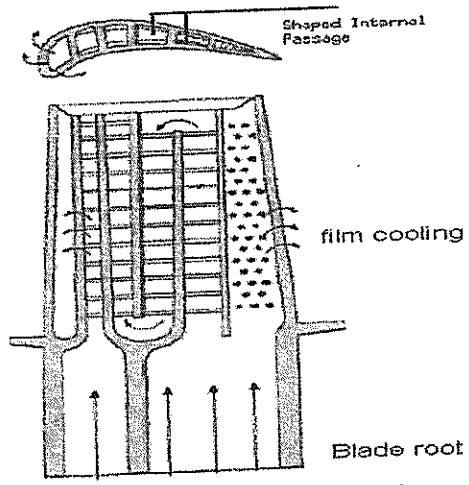

Fig.(23) Combined film and convection cooling.

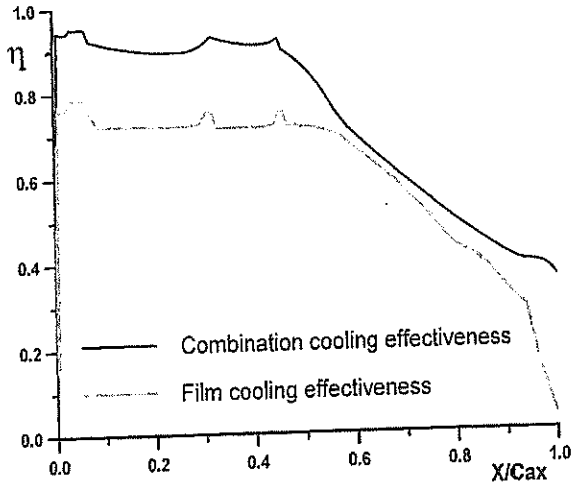

Fig.(24) Cooling effectiveness for film cooling as well as combined film and convection cooling, Tu = 5 and Br = 0.08.

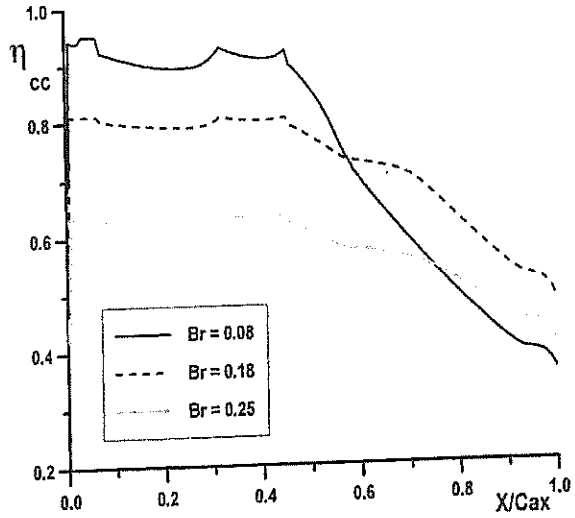

Fig.(25) Effect of blowing ratio on combined film and convection cooling, Tu = 5.

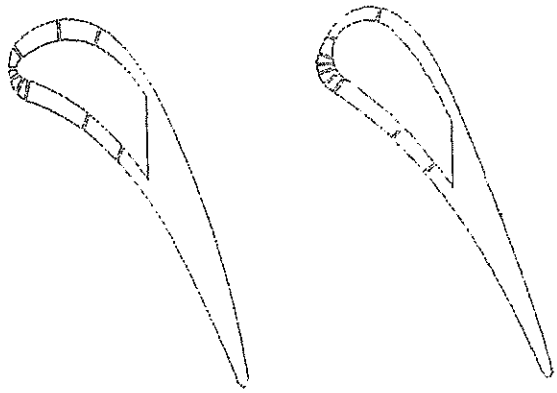

VKI cross-section C3X cross-section

Fig.(26) Geometry of gas turbine blade.

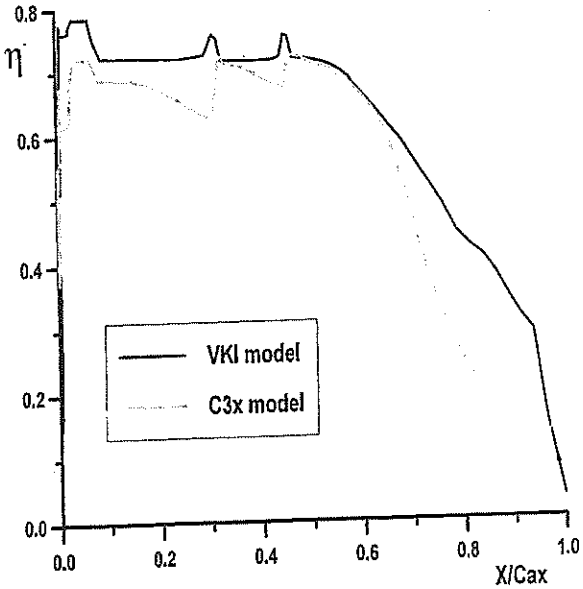

Fig.(27) Effect of blade shape on the film cooling effectiveness distribution, Tu = 5 and Br = 0.08.

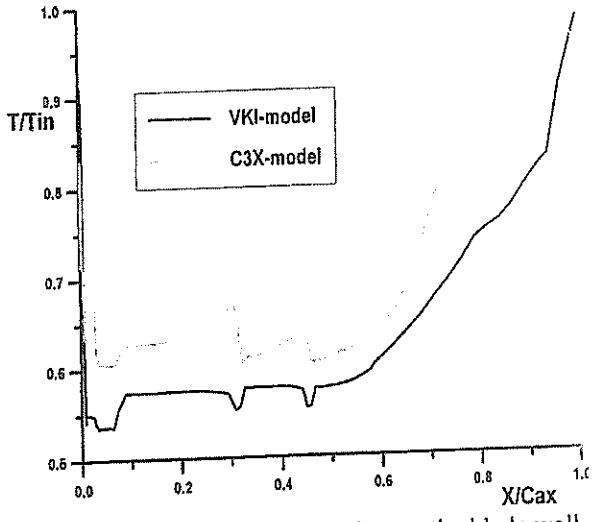

Fig.(28) Temperature distribution on the blade wall, Br = 0.08, Tu = 5 %.

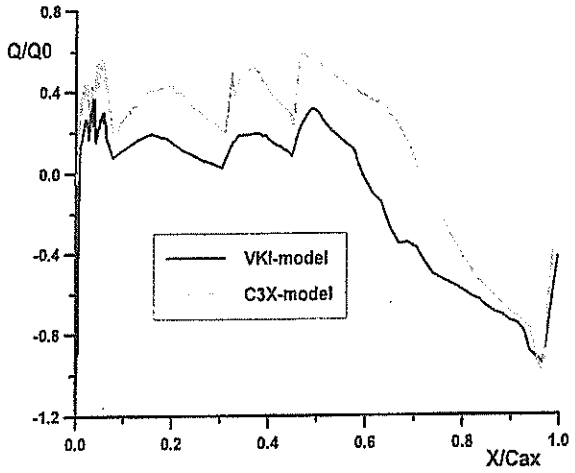

Fig.(29) External surface heat flux on the nozzle blade, Br = 0.08, Tu = 5 %.

Table 1 : Flow conditions for flow over plate

u_{in}	T_g	Tu	T_c	Br	Ma	α_j
30 m/s	290 K	5 %	345 K	1.0	1	90 °

Table 2: Blade design parameters

Air exit angle	70.96°
Throat diameter	39.83 mm
Blade height	76.20 mm
Blade spacing	129.7 mm
True chord	136.2 mm
Axial chord	68.53 mm

Table 3: Turbine blade flow conditions
$Ma_{ex} = 0.9$, $Re_{ex} = 1.56 \times 10^6$, Tu = 6.5 %

Run Code	T_w/T_g	P_g/P_{go}	P_{go} (Pa)	T_{go} (K)
Un cooled	0.78	0.6	273446	686.7

Table 4: Blade design parameters
Three staggered rows of cylindrical cooling holes (d = 0.8 mm; s/c = - 0.031, 0, 0.031) were located around the leading edge.

Blade true chord length (C)	80 mm
Blade axial chord length (C_{ax})	58 mm
Blade span (H)	48 mm
Blade pitch (Pi)	53.6 mm
Exit flow angle (B2)	70°

Table 5: Turbine blade flow conditions
$Ma_{in} = 0.251$, $Ma_{ex} = 0.905$, $Re_c = 8.42 \times 10^5$, Tu = 5.2 %

Case	P_{go} (Pa)	T_{go} (K)	T_w/T_g	T_c/T_g	m_c/m_g
120	289500	409.5	0.727	0.52	0.62 %